3D-Morphology of the central membrane for a new concept of fuel cell

Keywords: fuel cell; ionic conductivity; tridimensional pore network; water diffusion.

I. Context of the study

High temperature fuel cells are promising systems to electrochemically generate electricity and heat for stationary applications. Fuel cells provide many advantages over traditional energy conversion systems including high efficiency, reliability, modularity, fuel adaptability and very low levels of polluting emissions. Among them, the most mature device is the Solid Oxide Fuel Cell (SOFC) which essentially consists in two porous electrodes separated by a fully dense oxide-ion conducting electrolyte (figure 1b). The operating principle of such a cell is illustrated in figure 1. Oxygen supplied at the cathode side of the cell reacts with incoming electrons from the external circuit to form oxide ions, which migrate to the anode through the electrolyte. At the anode side, oxide ions combine with hydrogen in the fuel to form water, liberating electrons. Electrons flow from the anode through the external circuit to the cathode. Nevertheless, SOFCs are in a very early stage of their commercialization due to several technical drawbacks caused by the high operating temperature (generally > 900 °C) imposes by the electrolyte. Lately, different approaches have been developed in order to decrease the SOFC's operating temperature. One of them is the development of the Proton Conducting Fuel Cell (PCFC), a concept based on new type of charge carriers (H^+ instead of O^{2-}) (figure 1a). Since protons conduction requires lower energy than oxygen ions, this type of fuel cell is able to operate at lower temperatures, typically in the range 500-700 °C.
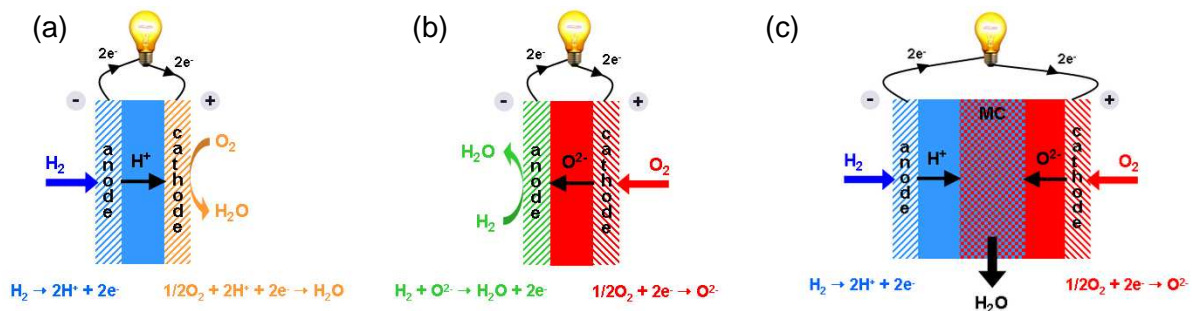

Figure 1. Rough sketch of (a) a PCFC, (b) a SOFC and (c) the IDEAL-Cell concept.

However, both concepts present limitations related to the concepts themselves. In the case of SOFCs, water formation occurs at the anode side which is responsible for fuel (hydrogen) dilution and then decreases the activity of the electrocatalytic sites where hydrogen oxidation takes place. On the other hand, in PCFCs, water is formed at the cathode side which not only decreases electrocatalytic activity but most of all creates a highly corrosive mixture of water, oxygen and high temperature which is very demanding for the materials. In order to overcome limitations of the two already existing systems, a new concept of fuel cell has been proposed by the Centre des Matériaux of Mines ParisTech. This one (figure 1c) consists in joining the anode side of a PCFC (figure 1a) and the cathode side of a SOFC (figure 1b) through a central membrane (CM). Therefore, protons are created at the PCFC anode and are diffused through the electrolyte towards the CM while oxygen ions are created in the SOFC cathode and also diffused through an electrolyte towards the CM. Then, protons and anions combine to form water which is eliminated. This new concept of fuel cell is being developed by a European research consortium constituted by 9 partners both academic and industrial coming from five different European countries (France, Germany, Italy, Poland and Bulgaria). This project was financed by the European Commission under the Seventh Framework Programme – theme Energy (FET, 2008-2011). The concept has been patented by the consortium leader.

II. CM prerequisites

The CM of IDEAL-Cell is the core and critical element of the concept and then the truly innovative step in this fuel cell concept. It is a porous medium made of both the anion (ACP; YDC15) and the proton (PCP; BCY15) conducting phases. As the reaction of water formation (recombination of H^+ and O^{2-}

ions) takes place within the CM, its composition and morphology must be optimized for this basic purpose. As the proton conductivity in the PCP is expected to be much higher than the oxygen conductivity in the ACP at a given temperature, so that the optimized composition is not a priori the one for which the two active phases are in the same volume proportion. The volume fraction of both ACP and PCP is a parameter to considered since it offers an efficient lever to tailor the location where the reaction for water formation will take place in the CM; it is thought that the delocalization of this reaction toward the ACP electrolyte should allow giving room to integrating a channel pattern toward the PCP in view of an efficient water evacuation.

Moreover, all morphological parameters such as porosity and particle size and shape, tortuosity, percolation and permeability will influence the charge transport carrier and the water flow within the CM. There must be morphological sites where the three phases meet and in which ACP and PCP percolate towards their respective electrolytes, and porosity must percolate towards the outside of the cell (figure 2). However, the percolation of the TPBs is not requisite, which strongly releases the percolation conditions that prevail for the electrochemical reactions taking place in SOFC and PCFC electrodes. As the volume density of TPBs has a straightforward impact on the number of reactional sites where the water formation occurs, the more TPBs, the more the local volume-specific reaction rate and the more the exchange current density within the CM.
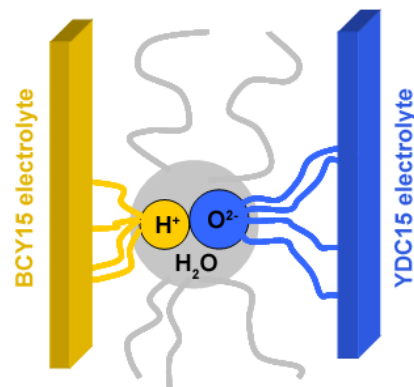

Figure 2. Scheme of the ionic and porosity percolation pathways within the CM.

In our case, two major aspects have to be considered about the design of the CM: (i) the reactive volume, represented by the TPBs must be extended to its whole volume and (ii) an effective evacuation of water must be ensured. Effective water evacuation will depend on the pores size and their tortuosity and percolation inside the CM. In fact, high porosity may not be enough for the CM's efficient performance if pores do not percolate in order to create pathways that allow water evacuation from the bulk towards the exterior. Moreover, water evacuation might be limited if tortuosity of pathways is far from unity, generating highly curve porosity wherein water can condense. A quantitative analysis of back-scattered scanning electron microscopy (BS-SEM) cross section image was carried out but it doesn't give useful information about the interconnected pore network (figure 3). Pores that may seem closed in the 2D image can actually percolate thorough the missing dimension on the image.
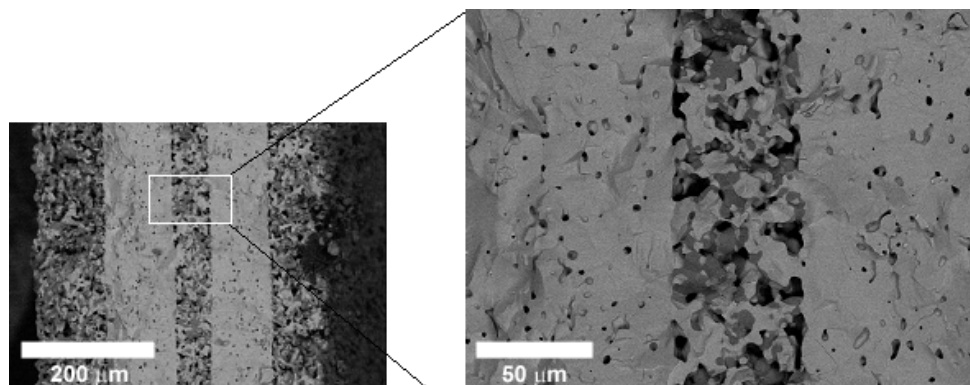

Figure 3. SEM cross-section of the CM in a 5 layer structure obtained by tape casting and co-sintering.

Therefore, knowledge of the real 3D morphology of the CM is of primary importance to model the fluid's flow and the membrane's electrical properties and consequently optimize its performance based on its microstructure and shaping process parameters. For these reasons, we propose to use the ESRF facilities to carry out the 3D characterization of this CM microstructure by X-ray microtomographies. These experiments were carried out according to two session, first to study the reactive volume in the CM where the electrochemical reaction of ions recombination takes place to form water (17th-18th July, 2009) and second to explore channed structures for an effective evacuation of this latter (19th-21st October, 2010).

III. Results from the first session: 17th-18th July, 2009

III.1. CM sample preparation

In order to study in 3D the morphological parameters (porosity size and shape, porosity, percolation…) that were identified by modelling as having strong influence on the electrical efficiency of the IDEAL-Cell, a set of CMs were produced for microtomography experiment, varying:

- The volume fraction of porosity: figure 4 clearly shows that this parameter can be easily controlled through an appropriate quantity of pore former. 3 amounts, 40%, 50% and 60%, were chosen in the present study;
- The nature of the pore formers (figure 5), poly-vinyl-butyral (PVB), graphite and corn starch in order to control the pore shape and size after sintering (figure 6);
- The volume ratio between the proton conducting (PCP, BCY15) and the anion conducting (ACP, YDC15) phases: 40/60, 50/50 and 60/40 ratios were selected here.
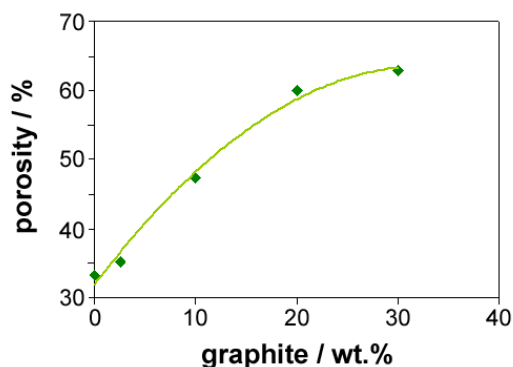

Figure 4. Evolution of the porosity in the CM as a function of the graphite content.

Figure 5 displays micrographs of the powders used to design the pore within CM. Obviously, subsequent to sintering, the size and morphology of the residual pores will be directly related to the nature of the pore former used. As an illustration, an aggregated and almost spherical particles containing powder (corn starch; figure 5c) gives rise to sphere-shaped pores as observed in figure 6c.
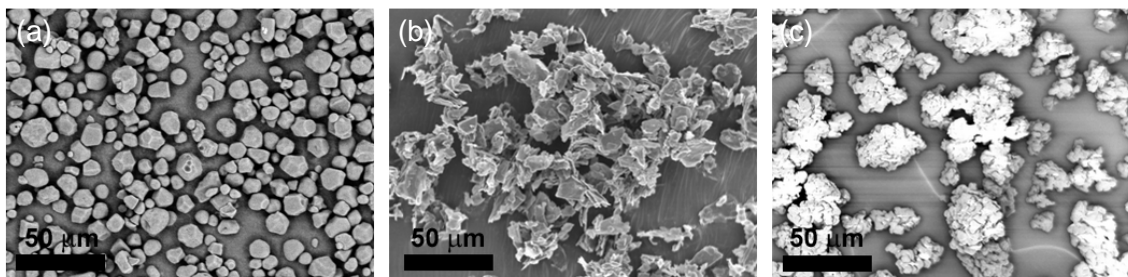

Figure 5. Different pore formers used for the preparation of the CM; (a) Poly-Vinyl-Butyral, (b) graphite and (c) corn starch.
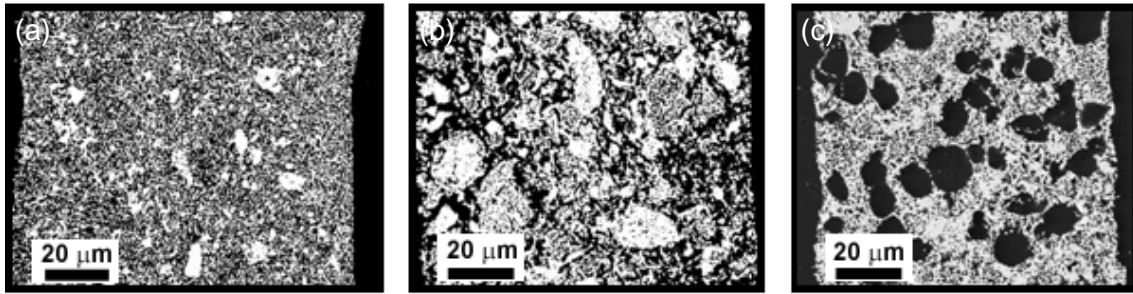
Figure 6. SEM images of CMs cross sections for which different pore formers were used: (a) Poly-Vinyl-Butyral, (b) graphite and (c) corn starch.

These single-layered CM were then characterized by X-ray microtomography at the European Synchrotron Radiation Facility (ESRF) at Grenoble, France (July 17th and 18th, 2009). Experiments were carried out on the beamline N°19 dedicated to "microtomography and phase contrast" requirements.

III.2. Experimental conditions

III.2.1. Microtomography

The principle of microtomography is very similar to that of the well-known medical scanner. It consists in recording a series of radiographs at different angular positions of the sample, which rotates around an axis perpendicular to the highly energetic X-ray beam. The best images, in terms of spatial resolution, signal-to-noise ratio and quantitative exploitation, are obtained when a synchrotron radiation is used under high intensity, practically parallel and monochromatic incoming beam conditions. The range of pixel sizes available at ESRF goes from 0.30 to 30 µm.

III.2.2. Phase contrast imaging

The X-ray beams produced at third generation synchrotron radiation facilities exhibit a high degree of coherence that allows recording "phase images" by varying the sample-to-detector distance. An increased sensitivity is provided that allows identifying materials with neighbouring densities (for example Al and Si, and in our case BCY15 and YDC15).

A significant number of samples were tested (27 CMs gathering 3 volume fractions of porosity, 3 compositions [ratio PCP/ACP] and 3 different pores formers); the best possible results at the highest spatial resolution that the technique could allow were obtained. 1200 tilt series were obtained for each sample, which will allow easily reconstructing the whole volume (an example is given in figure 7).

The best recording parameters are dependant on the:

- Nature of the sample holder;
- Incident beam energy that allowed reducing background noise to signal ratio keeping the contrast between the three BCY15, YDC15 and porosity phases;
- Signal acquisition time.

The best conditions which were retained were:

- The sample was pressed between the chaps of a stainless steel sample holder (figure 8c) to eliminate vibration;
- Distance between the camera and the sample: 10 mm;
- Incidence beam energy: attempts were made using also energies of 30.0, 38.0, 40.0 keV in order to maximize the contrast between both BCY15 and YDC15 phases and to reduce the noise to signal ratio. The best compromise was 22.5 keV;
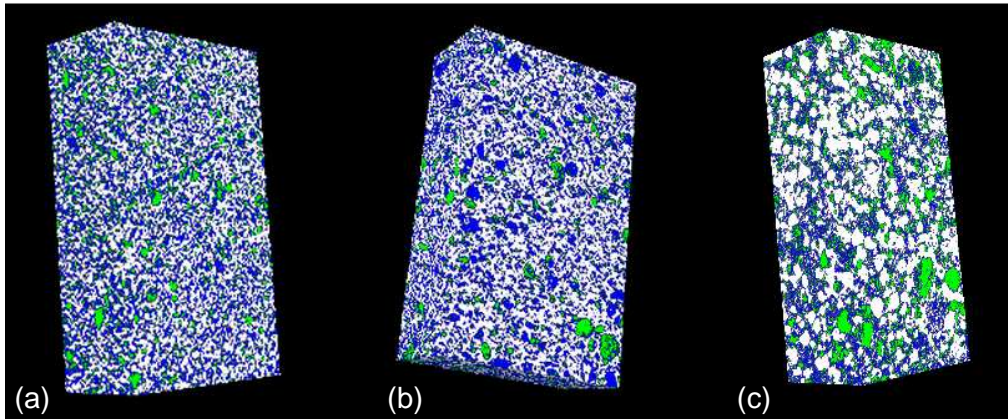- Total recording time was 1 hour per central membrane sample.

Figure 7. First images of the 3D reconstruction of CM samples showing BCY15 (green parts), YDC15 (blue parts) and the porosity (white parts). Three pore formers were used, (a) Poly-Vinyl-Butyral, (b) graphite and (c) corn starch.

<u>III.2.3. Reasons which justified the choice of experimental conditions</u>

Through previous scanning electron microscope analyses (figure 6), pore sizes between 1.0 and 15 µm were estimated. Therefore a resolution of 0.28 µm pixel^{-1} was required, which imposed the use of samples with 300 µm × 300 µm cross sections (whatever the length). As samples of the CM are highly porous (> 40% of relative porosity), hence easily breakable, tape casted and sintered layers were first impregnated with an epoxy resin and carved in fine slices having the dimensions mentioned above.

The first sample was prepared by putting down its tip on a stainless steel support (figure 8a), whose surface was made sticky by means of resin (figure 8b). Nevertheless, the 2D images recorded were blurred because of vibration of the sample originating from the degradation of the resin under the highly energetic X-ray beam. A stainless steel sample holder was then selected successfully for all experiments insofar as high quality images were recorded.
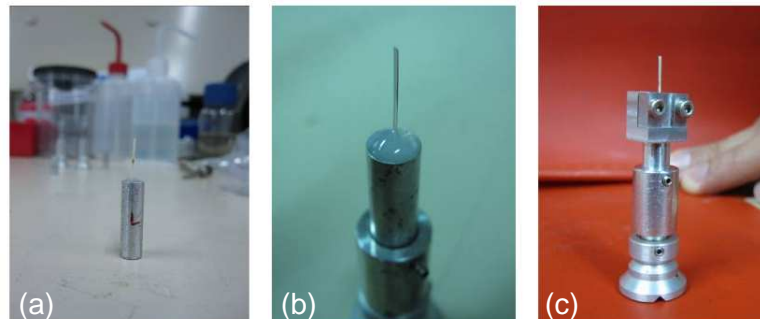

Figure 8. Different sample holder selected for the X-ray microtomography experiments.

The beam energy (22.5 keV) was chosen so that the two materials present the highest difference in X-ray absorption with the lowest possible background noise (see figure 9).
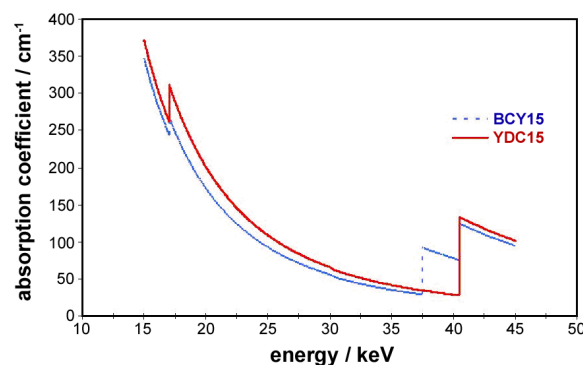

Figure 9. X-ray absorption coefficient as a function of the beam energy for PCP (BCY15) and ACP (YDC15).

5

III.3. Image processing

III.3.1. Image segmentation

After a first analysis of the images obtained at ESRF, it was decided not to work with the samples for which Poly-Vinyl Butyral was used as a pore former because the pores were too small for an accurate segmentation of 2D images. In the end, data for ten samples were used, five with corn starch and five with graphite as pore formers. Each of the phases (BCY15, YDC15 and porosity [replaced by the epoxy resin for the experiments]) had different X-ray linear absorption coefficients and therefore each of them presented different grey levels that allowed their segmentation by applying the correct threshold.

As it had been expected from the absorption coefficient data (figure 9), the proton conducting phase (PCP; BCY15) is brighter than the anion conducting phase (ACP; YDC15). Porosity was filled with an epoxy resin and appears black in the images. After obtaining the first segmentation (see figure 10), it appeared that at the interface between the pores and the brighter phase, voxels with an intermediate grey level were detected and then attributed to the anion conducting phase (YDC15). This effect created a fake ring around the brighter phase wherever it was in contact with a pore, as one can see in figures 10a and 10b. The presence of this ring was keeping the proton conducting phase from percolating in the first measurements that were made.
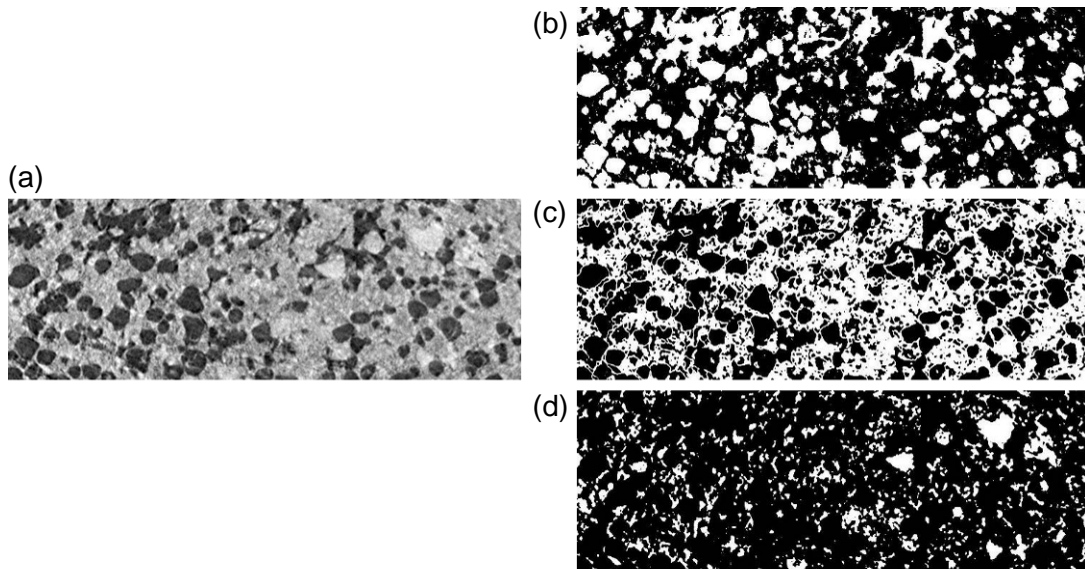

Figure 10. Image segmentation for a sample with corn starch as pore former: (a) original image, (b) porosity, (c) anion conducting phase and (d) proton conducting phase.

A sequence of image processing operations was determined in order to eliminate this artefact. The final result is shown in figure 11c, and as it can be seen the interfaces are noisy and unrealistic due to the former operations. A new sequence of image treatment operations was determined to smooth the surfaces. Each one of the phases was then properly obtained and to each one of them a grey level was attributed (figure 11d).
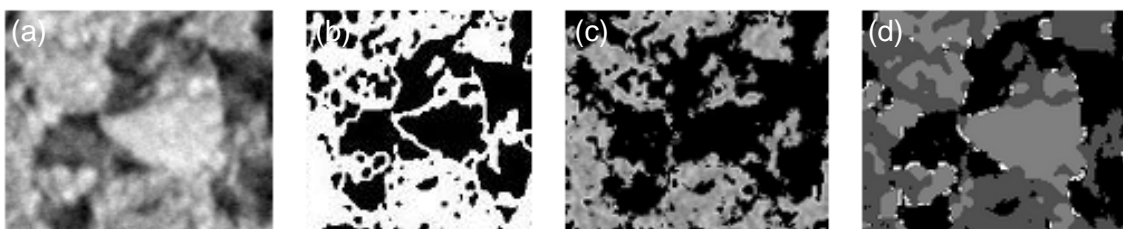

Figure 11. Detail of an image obtained by X-ray microtomography: (a) original image, (b) first trial for anion conducting phase segmentation, (c) anion conducting phase after image treatment to remove an image detection artefact, (d) final image with the three phases identified.

III.3.2. Extraction of active triple phase boundaries segments

After identifying the three phases for each sample, active TPBs were extracted. The algorithm used allows identifying the proton and oxygen ion conducting phases in the neighbourhood of porosity. The intersection of the three phases yields the total triple phase boundaries segments (figure 12).
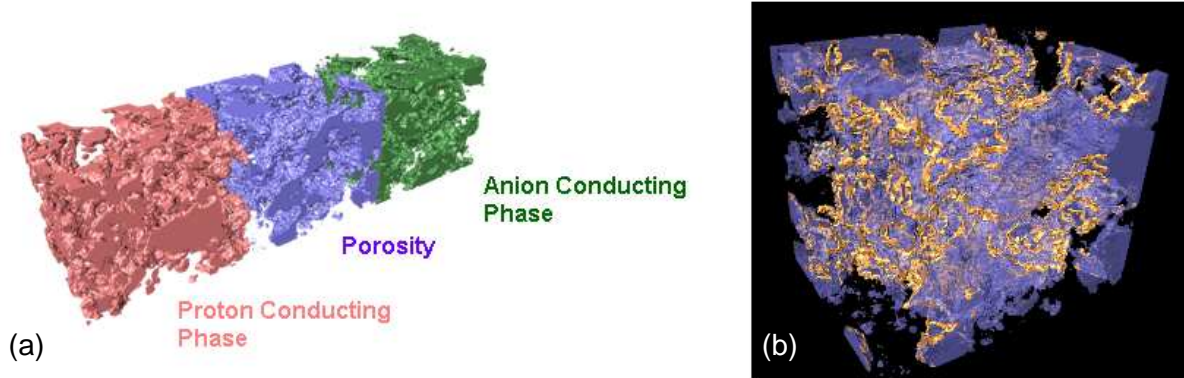

Figure 12. Extraction of (a) the three phases and (b) total triple phase boundaries of a sample for which corn starch was used as pore former.

The detection of the active TPBs required to identify:

-   The voxels of proton conducting phase (PCP; BCY15) connected to the anode;
-   The voxels of the anion conducting phase (ACP; YDC15) connected to the cathode;
-   The voxels of porosity (epoxy resin) connected to the exterior of the central membrane.

These voxels will be the ones reached by a geodesic propagation coming from the surface to which they must be connected. For example all the voxels of the proton conducting phase reached by a geodesic propagation coming from the anode are considered to be connected to it through a path in that phase. The intersection of the three phases gives the segments where the three phases are in contact and each of them percolates to the anode, cathode or exterior of the cell. If we intersect these segments with all the TPBs previously identified, we obtain the active TPBs. The percentage of active TPBs and their length was determined for all of the samples (table 1).

Table 1. Percentage of active triple phase boundaries segments and respective length.

Sample	Design.	BCY15/YDC15 / vol.%	Porosity / vol.%	% active TPBs	Active TPBs length / m mm^{-3}
1	A	40/60	40	56	563
2	C		60	54	607
3	D	50/50	40	39	563
4	H	60/40	50	47	292
5	I		60	63	441
6	K	40/60	50	52	981
7	L		60	75	901
8	M	50/50	40	64	910
9	O		60	58	671
10	R	60/40	60	64	748

J.R. WILSON *et al.* published an article in which they reported results of 3D reconstruction of an SOFC anode using SEM-FIB at higher magnification and images analyses. They have found 63% of active triple phase boundaries and a specific-volume length of 4.28×10^3 m mm^{-3}. Therefore the first results obtained here on non-optimized microstructures can be considered as realistic[1].

---

[1] J.R. Wilson *et al.*, Three-dimensional reconstruction of a solide oxide fuel-cell anode, Nature Materials, Vol. 5, July (2006).

III.3.3. Phase percolation and tortuosity

After extraction of the three phases and triple phase boundaries, percolation rates and tortuosities were determined in the x, y and z direction for each one of the phases. The algorithm implemented to determine percolation applies geodesic propagations into the studied media along the forward and backward directions using a sphere as a structural element. Only the paths that reach the opposite face of the volume in both directions are extracted. For each one of the voxels belonging to the percolating pathways, tortuosity is determined as the ratio of the geodesic distance of the path connecting two opposite faces that passes through that voxel, to the Euclidean distance between the two surfaces (figure 13).
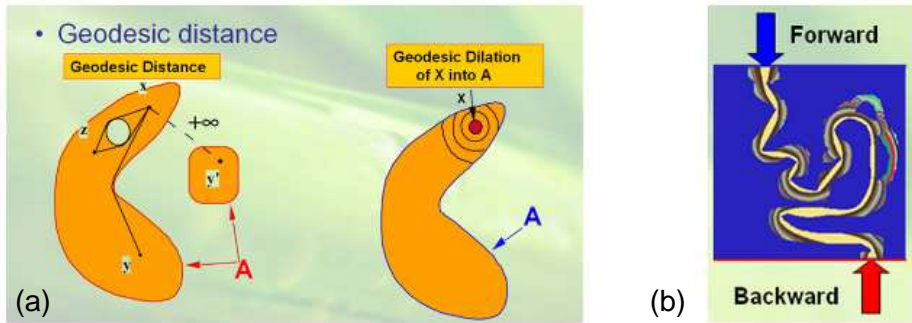

Figure 13. (a) Definition of geodesic distance and (b) geodesic propagation in a porous medium.

Therefore we obtain not a single value of the tortuosity for a porous structure but an histogram of tortuosities for the voxels that belong to a percolating path. In figures 14 and 15 are shown two examples out of the ten samples that were analysed. Through the results one can conclude that for both types of samples we obtain very high percolating ratios – always above 93% – for the three phases. The percolating paths created are very straight for the solid and gas phases with tortuosities close to one,which means that the path length is very close to the Euclidean distance which is very suitable for charge and mass transportation in the central membrane. On the other hand triple phase boundaries segments have a rather high tortuosity of about 2.5, which indicates that they are far from being straight; this is totally appropriate for an increased length of active TPBs.

III.3.4. Prediction of the effective properties of the CM

The Centre de Morphologie Mathématique (CMM) of Mines ParisTech developed a software that allows to predict the physical properties of materials from images of their microstructure. It is based on the 3D computation of fields from 3D images, based on iterations of fast fourier transforms (FFT). On the occasion of the IDEAL-Cell project, it is therefore possible to give the following estimations for which preliminary results were obtained:

- 3D prediction of the Darcy's permeability tensor by FFT resolution of the Stokes equations;
- Conductivities (anionic and protonic).

A first estimation of the Darcy permeability for water of the sample represented in figure 7 was obtained in one direction of propagation of the fluid (Ox). Other directions should be considered, to account for the anisotropy of the porous medium. The estimated permeability gives $k = 1.35 \times 10^{-10}$, for a length in cm. This is similar to the permeability of sandstone (in the range 10^{-10}-10^{-11}). Similarly, a first estimation of the effective bulk conductivity of each component was obtained for samples C and I, and are given in table 2. They are obtained for the propagation of current in the same direction as for the flow of water. In this table, we give a relative effective conductivity,that must be multiplied by the absolute conductivity of the corresponding component.

Table 2. Relative effective anionic and cathodic conductivity in the Ox direction.

Phase, sample	Relative conductivity / S cm^{-1}
H^+ conductivity of sample C	0.0551
O^{2-} conductivity of sample C	0.0477
H^+ conductivity of sample I	0.0377
O^{2-} conductivity of sample I	0.0530

In a next step, further points will be developed:

- Estimation of the full tensor of permeability and conductivity;
- Estimation of the representative volume element (RVE) for each property;
- Validation of the results by comparison with available data, for the input of properties in the macroscopic models.

Finally, after calibration, it will be possible to use this approach for application to simulations of models of random microstructures, in order to optimise the effective properties with respect to the end properties of the IDEAL-Cell.
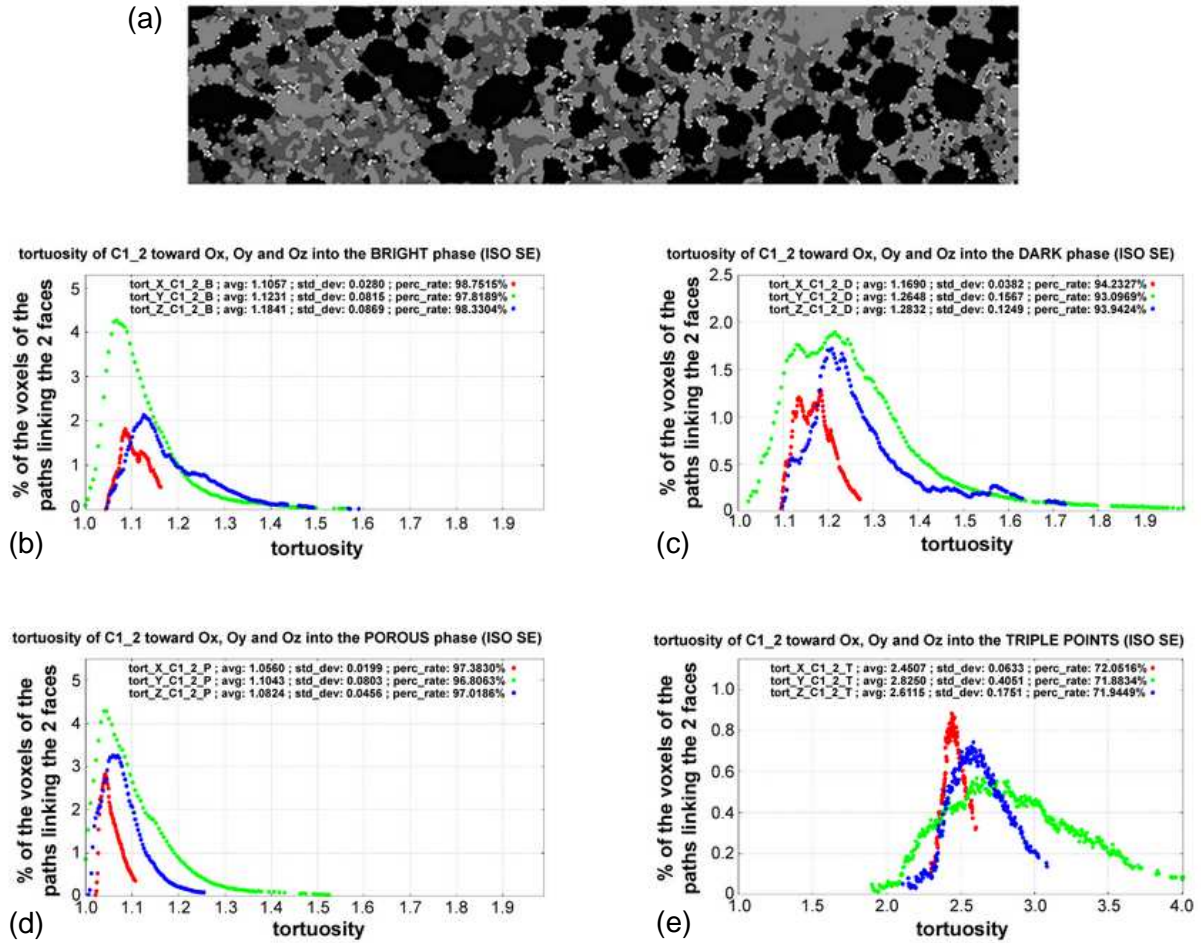

Figure 14. Results obtained for a sample for which corn starch was used as pore former: (a) 2D cross section with phase segmentation, (b) tortuosity histograms and percolation rates for proton conducting phase, (c) anion conducting phase, (d) porosity and (e) total triple phase boundaries.
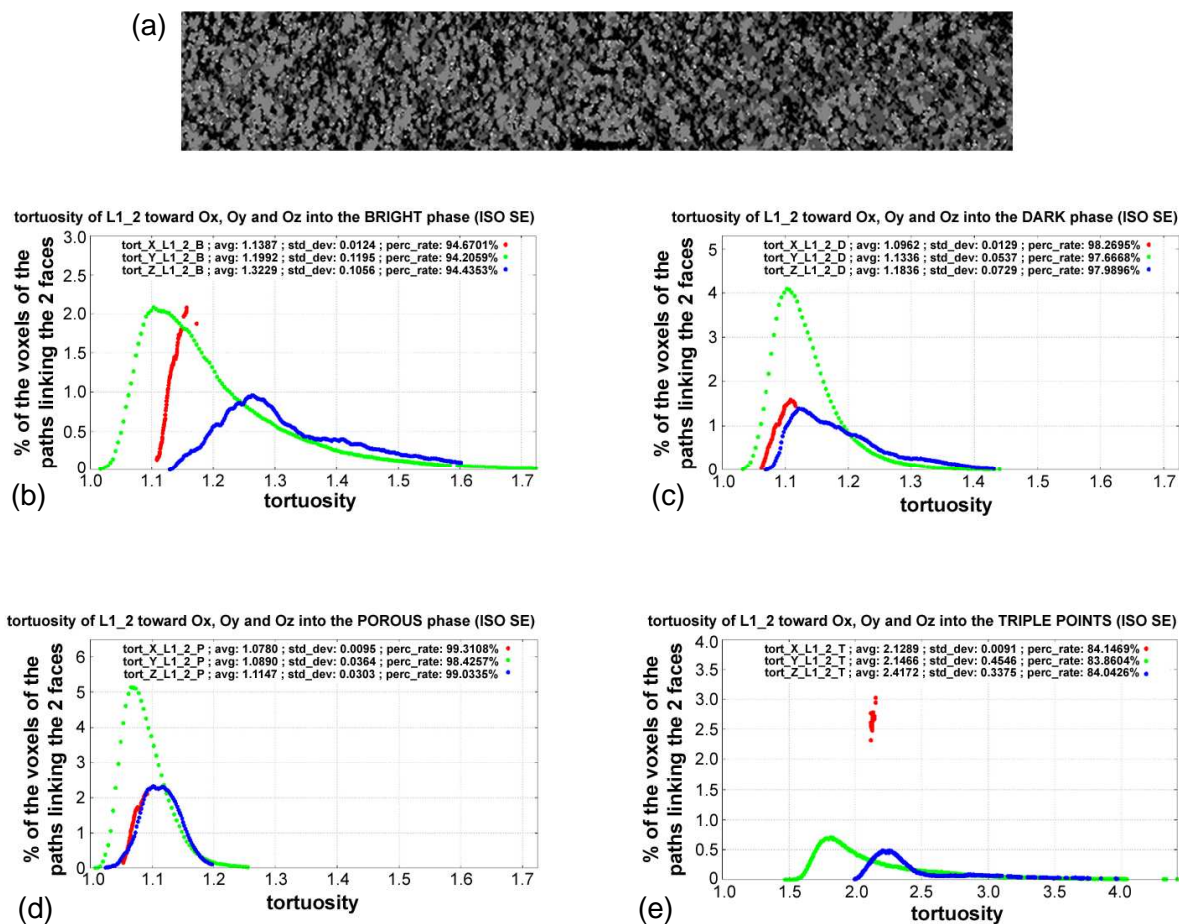
Figure 15. Results obtained for a sample for which corn starch was used as pore former: (a) 2D cross section with phase segmentation, (b) tortuosity histograms and percolation rates for proton conducting phase, (c) anion conducting phase, (d) porosity and (e) total triple phase boundaries.

IV. Results from the second session: 19th-21st October, 2010

In order to go further in the optimisation of the CM microstructure and especially to make water evacuation more efficient, a 3D cross-linked channelled architecture has been considered (using polymeric meshes) along with the existent already optimized microporosity, dispersed in the whole ceramic volume and generated by adding pore formers (see part III). These sophisticated samples, were prepared by dip coating and tape casting. The single-layered channelled CMs were then subjected to X-ray microtomography analyses at the ESRF in Grenoble, France (October, 19th-21st October, 2010). Experiments were carried out on the high-resolution diffraction topography beamline (ID19) dedicated to "microtomography and phase contrast" requirements.

IV.1. Channeled CM sample preparation

A significant number of samples were scanned and are listed below:

- 40 single layer CMs prepared by dip coating including 5 different meshes from SEFAR and 3 different pore formers;
- 18 single layer CMs produced by tape casting gathering 5 volume fraction of porosity, 3 compositions (different ratio between BCY15 and YDC15 active phases), 3 different pore formers and 6 thread mesh diameters;
- 6 "monolithic" CMs (as references), produced by tape casting, and containing only BCY15 with varying "standard" and channelled porosity. These samples were studied with the aim at integrating them into a monolithic IDEAL-Cell concept in which TPB segments are replaced by TPB suface (significant increases of active sites, decreases of polarization resistance…) as only one phase consitutes the CM.

<u>IV.1.1. Channeled CM prepared by dip coating</u>

First dip coating experiments to fabricate CM samples with channelled microstructures were performed with the aim at ensuring an effective evacuation of water produced. A novel, simple and cost effective method was recently reported by J.C. Ruiz-Morales et al.[2], based on dip coating for the creation of a 2D/3D matrix of cross-linked channels through SOFC electrode materials. This method was adapted here to produce IDEAL-Cell CM samples with optimized microstructure, in favour of water removal, by means of successive optimization of operating conditions. The experiment consists in dipping a polymeric net (PET-based mesh) in a freshly prepared slurry made of the oxide powder(s) and organic additives. In most cases, one single immersion is sufficient to get complete coating of the polymer fabric. After drying at room temperature (RT) the coated net can be easily shaped into any geometry, cut out (as a disk, square base parallelepiped, etc…), bent or rolled. The final step is a slow firing process, which helps removing all organic materials producing the desired porous channels. In figure 16, the sketch of the experiment is reported.
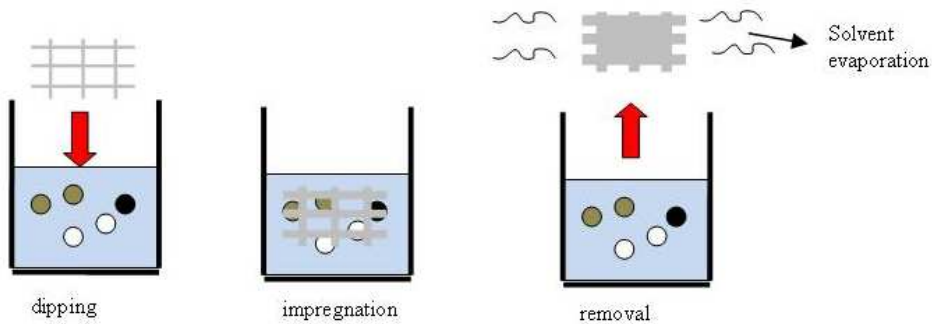

Figure 16. Sketch of dip coating experiment showing the succession of processes.

Obviously, the idea consists in implementing a cylinder-shaped channel network into the optimzed porous microstructure (high density of TPBs, percolating phases…) of the CMs; the use of pore formers (commercial starch or graphite) is then still relevant to create the porous matrix. Table 3 and figure 17 report details (including grain shape and size) about the different pore formers used. As starting composition, a slurry based on the mixture of 50% BCY15 and 50% YDC15 in volume was prepared. With a view of simplifying shaping process for fabrication of IDEAL-Cell (avoiding composition variation from one layer to the other) while increasing its electrochemical performances, the use of the BCY15 material only was considered. Indeed, it has been demonstrated, in the frame of our research that BCY15 exhibits both anionic and protonic conductivities, that tend to equalize at 600 ℃; then, it appears judicious to totally replace Y DC15 by BCY15 to form the BCY15 / CM-BCY15 / BCY15 succession of layers. Therefore, BCY15 based slurries were also prepared.
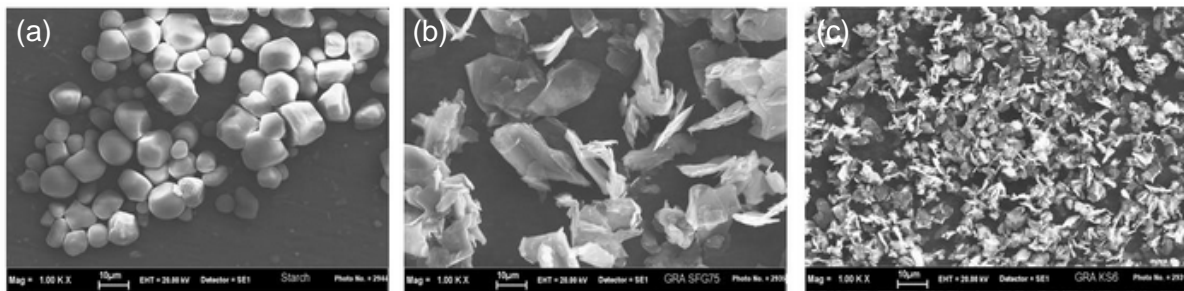

Figure 17. Pore formers, (a) starch, (b) graphite SFG75 and (c) graphite KS6.

In order to obtain stable slurries leading to a green layer with good rheological properties after dip coating, some additives must be added and mixed together with powders: as solvent, a mixture of methyl-ethyl-ketone and ethanol (3/2 w/w) was used while the dispersion is assumed by the addition of mono and di-phosphate esters (MONOFAX 057). Polyethylen glycol (PEG 400) and polyvinyl butyral (PVB) were finally added as plasticizer and binder respectively. Table 4 report the detailed composition of the slurry. After each component addition, the slurry was thoroughly ball milled in a

[2] J. C. Ruiz-Morales, J. Pena-Martinez, J. Canales-Vasquez, D. Marrero-Lopez, C. Savaniu, P. Nunez. J. Am. Ceram. Soc., 92 [1] 276–279 (2009).

PET bottle with small zirconia balls for 2 hours. After separating out the balls of the mixture by filtration, the slurry is ready for coating.

Table 3. Morphological and granulometric characteristics of the pore formers used.

Type	Nomenclature	Size / µm	Shape
Starch from Aldrich	S	> 10	spherical
Graphite KS6 from Timrex	GS	d_{90} = 5.8-7.1	lamellar
Graphite SFG75 from Timrex	GB	d_{90} = 53-67	lamellar

Table 4. Summary of slurry composition.

Component	Quantity
Powder	10.0 g of BCY15 or 5.23 g YDC15 + 4.77 g BCY15
Pore Former	0, 20, 40, 50 vol.% Starch, Graphite SFG75 and Graphite KS6 respectively
Solvent	8.0 g of methyl-ethyl-ketone/ethanol (3/2 w/w)
Dispersant	0.50 g of MONOFAX 057, mono and di-phosphate esters
Plasticizer	1.5 g PEG 400
Binder	1.0 g PVB
Mixing	Ball milling for 2 hours after the addition of each component

Obviously, the thickness of the prepared samples (mesh + slurry) is driven by the mesh thickness. Therefore, the use of thicker polymeric nets will lead to thick central membranes. In order to explore different central membrane samples, in terms of thickness and micro-channels diameter, five types of commercial nets were used, the diameter of channels being imposed by the thread diameter of meshes (table 5 and figure 18).

Table 5. Characteristics of the nets from SEFAR.

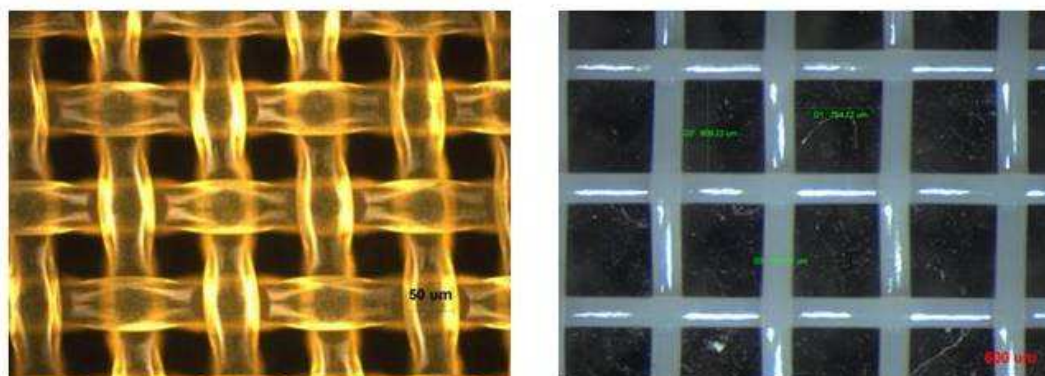| Commercial name	Nomenclature	Mesh opening / µm	Thread diameter /µm	Mesh thickness /µm
10/25-260	260	793	260	498
21/54-140	140	333	140	250
34/86.100	100	185	100	173
62/158.64	64	90	64	94
90/230-48	48	55	48	78

Figure 18. Structure of Mesh 48 (on the left) and 260 (on the right).

After dip coating of polymeric nets into the slurry, green samples were dried in air for 2 hours and then sintered with the following cycle: 400 °C for 4 hours with a 1 °C min^{-1} heating rate (to slowly remove organic additives and eventually starch), 650 °C for 2 hours keeping the previous heating rate (to oxidize graphite when present, otherwise skipped), 1250 °C for 5 hours reached with a 2 °C min^{-1} heating rate (sintering step), and cooling down to room temperature at 3 °C min^{-1}. Altogether, 40 samples (3×3 cm^2 and variable thicknesses) were prepared whose composition are reported in table 6. For ESRF experiments, dedicated 3×3 cm^2 samples are needed and were cut to appropriate sizes (parallelepiped with a square base of 300×300 µm^2) with the following procedure:

- embedding in epoxy resin;
- slicing by a diamond saw of 0.2-0.3 mm cuts;
- manual removing of resin by using an hot cutter blade.

The use of a resin is beneficial both to handle samples during cutting procedure avoiding to fall down the microporous channeled structure, and to guarantee a sufficient hardness during the X-ray data collection (indeed, it must be taken in account that the samples are fragile due to the channelled structure). The procedure of resin extraction is schematized in figure 19 below.
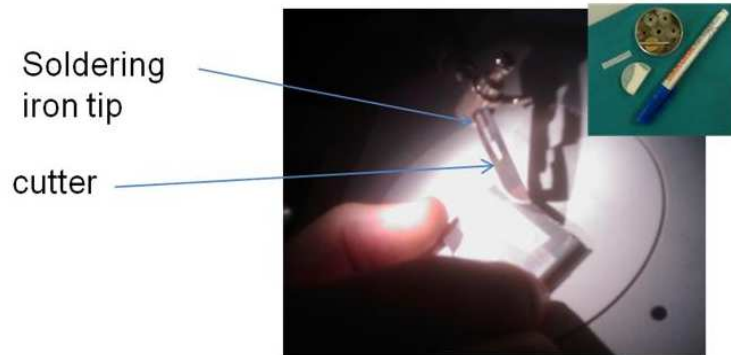

Figure 19. Cutting of 300 × 300 μm² sample for ESRF experiment. Manual removal of resin. In the insert slices obtained by diamond saw are reported.

Table 6. Summary of prepared samples using different type of meshes and amount of pore formers.

#	Name	Mesh used	Pore former type and amount added to (BCY15 + YDC15)
1	BY_S50_48	48	50 vol.%starch
2	BY_GB40_48	48	40 vol.%graphite SFG75
3	BY_GB40_64	64	
4	BY_GB40_100	100	
5	BY_GB40_140	140	
6	BY_GB20_140	140	20 vol.% graphite SFG75
7	BY_GB20_64	64	
8	BY_GB20_48	48	
9	BY_S20-140	140	20 vol.% starch.
10	BY_S20-100	100	
11	BY_S20-64	64	
12	BY_S20-48	48	
13	BY_S40_140	140	40 vol.% starch
14	BY_S40_100	100	
15	BY_S40_64	64	
16	BY_S40_48	48	
17	BY_GS40_260	260	40 vol.% graphite KS6
18	BY_GS40_140	140	
19	BY_GS40_100	100	
20	BY_GS40_64	64	
21	BY_GS40_48	48	
22	BY_0_48	48	none
23	BY_0_100	100	
24	BY_0_140	140	
25	BY_GS20_100	100	20 vol.% KS6
26	BY_GS20_140	140	
27	BY_GS20_64	64	
28	BY_GS50_100	100	50 vol.% graphite KS6
29	BY_GS50_64	64	
30	BY_GS50_48	48	
31	BY_S50_140	140	50 vol.% starch.
32	BY_S50_100	100	

			Pore former type and amount added to (BCY15)
33	B_GS20_140	140	
34	B_GS20_64	64	20 vol.% graphite KS6
35	B_GS20_48	48	
36	B_S20_140	140	
37	B_S20_100	100	20 vol.% starch
38	B_S20_64	64	
39	B_GB20_48	48	20 vol.% graphite SFG75
40	B_GB20_100	100	

Perfectly flat samples, without any observable cracks on the surface, were obtained (see figure 20); thickness was quite homogeneous along the samples and strongly dependent on the mesh and slurry viscosity used. The diameter of channels formed during sintering exhibits a shrinkage of about 20% with respect to the initial thread diameter.
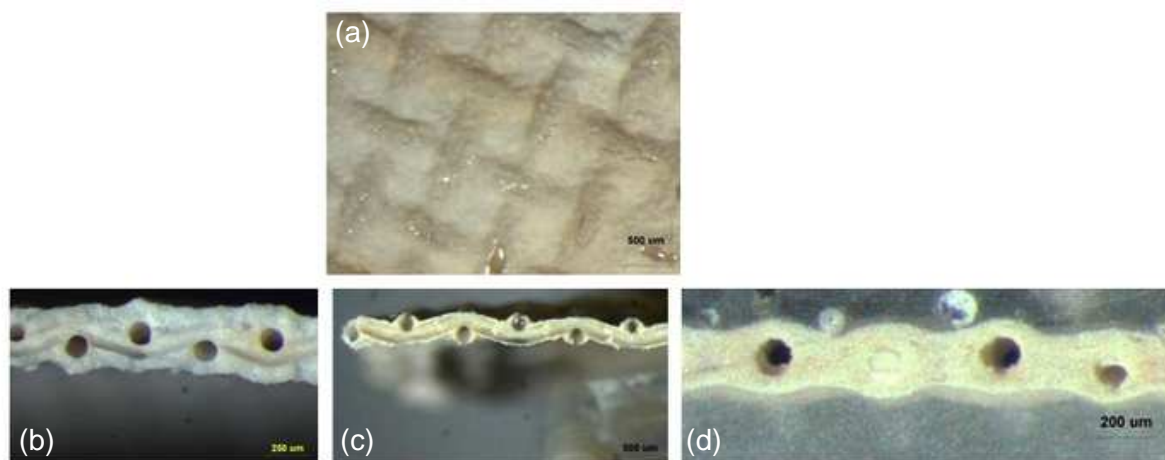

Figure 20. (a) BCY15-layer obtained using net 260, cross section of BCY15-layers obtained with (b) net 140 and (c) net 260 and (d) BCY15 + YDC15 + graphite-layer obtained using net 140.

In addition to channels, micro porosity is also distributed in the whole volume of the CM. In figure 21, the images recorded by SEM clearly show the effect of the nature of the pore formers on the resultant microstructure of the central membrane. In particular, the effect of graphite SFG75, graphite KS6 and starch is compared with the case where no pore former was added to the ceramic based slurry. This aspect is of particular importance because it could contribute significantly to the process of water evacuation. From EDS spectra, recorded on different zone of the samples (appearing in pink inserts, figure 21), no composition variation has been detected.

IV.1.2. Fabrication of CM samples by tape casting

Porous proton and oxygen ions conducting CM samples were prepared by tape casting and sintering, taking care of introducing polymeric meshes to create 3D cross-linked channels along with the micro porosity distributed in the whole volume of the sample. Obviously, the goal is to generate channelled porosity in samples for which the microstructure has been optimized.

IV.2. Experimental conditions

2048 tilt series were obtained for each sample, that allow easily for reconstructing the whole volume (an example is given in figure 22). The best recording parameters are strongly dependant on the:

- Nature of the sample holder;
- Incident beam energy that leads to the best compromise between a low background to signal ratio and a highly noticeable phases contrast;
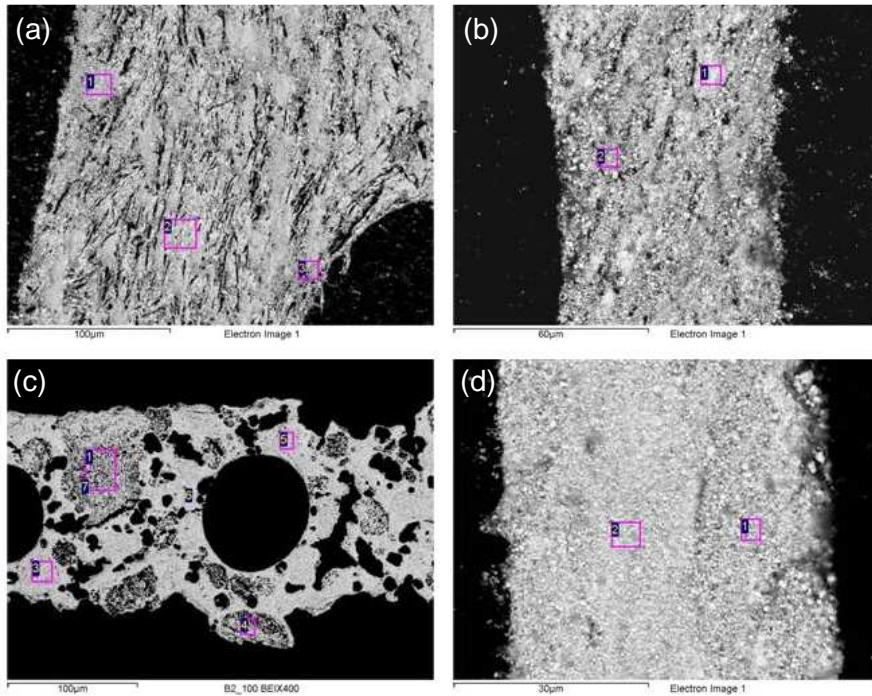- Signal acquisition time.

Figure 21. SEM images of microstructure of samples (a) prepared by adding 40 vol.% graphite SFG75 to BCY15 + YDC15 (50:50 in volume), net 260 was used; (b) prepared by adding 40 vol.% graphite KS6 to BCY15 + YDC15 (50:50 in volume), net 140 was used; (c) prepared by adding 20 vol.% starch to BCY15 + YDC15 (50:50 in volume), net 100 was used; and (d) prepared without any pore former, the composition of BCY15 + YDC15 being 50:50 in volume and net 140 was used.

Taking into account these considerations, the best conditions that were retained were:

- The sample, in the form of a stick (300 μm × 300 μm × whatever the length), is placed inside a thin Lindeman capillary of 0.1 mm in diameter whose internal surface was made sticky by means of paste;
- Distance between the camera and the sample was about 3-4 mm depending on tlit of the sample with respect to the vertical axis;
- An incidence beam energy of 30 keV was considered as the best compromise to maximize the contrast between both BCY15 and YDC15 phases, while reducing the noise to signal ratio;
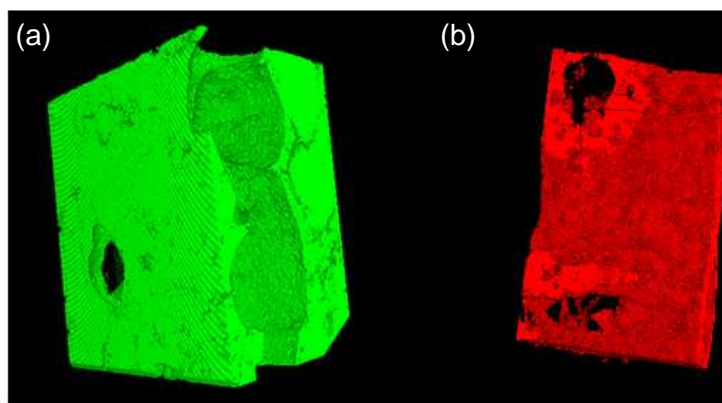- Total recording time was about 35 minutes per CM sample.

Figure 22. First images of the 3D reconstruction of channeled CM samples produced by (a) tape casting and (b) dip coating. The green and red colors are representative of the actives phases.

The reasons for which the experimental conditions were chosen are detailed in part III and were also considered in the course of this study. For such experiments, a high resolution is required and was fixed to 0.36 μm pixel^{-1}.

IV.3. Image processing

Each of the phases, i.e. BCY15, YDC15 and porosity (replaced by an epoxy resin), exhibits different X-ray linear absorption coefficients and therefore each of them displays different grey levels that allowed their segmentation by applying the correct threshold. As expected by the absorption coefficient data (figure 9), the proton conducting phase (PCP; BCY15) appears brighter than the anion conducting phase (ACP; YDC15) in the images (figure 23a). As for porosity that was filled with an epoxy resin, it appears black in the images. Therefore, the three phases can be identified by their different grey level.
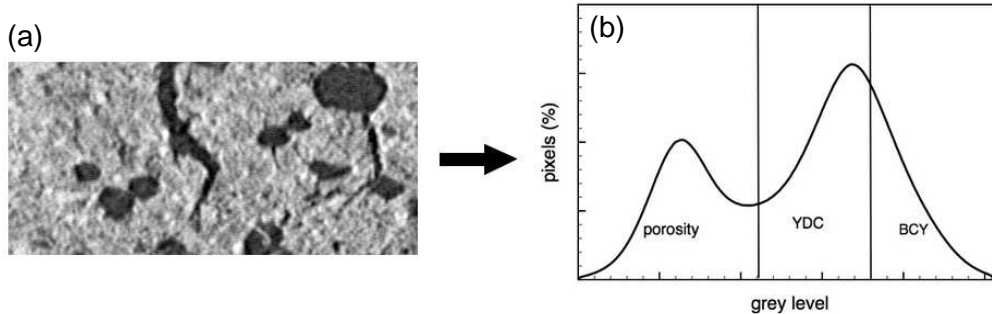

Figure 23. (a) Zoom in on a 2D image for a tape cast sample and (b) histogram displaying grey levels of the identified phases.

Regarding the histogram in figure 23b, displaying the grey level distribution in frequency, it becomes apparent that porosity (in black; figure 23a) and the ceramic materials (brighter in figure 23a) can be easily separated in the images: indeed, the two peaks are not convoluted. The porosity is systematically identified using an iterative algorythm[3]. Nevertheless, and we did not expect this difficulty to happen, there is only one local maxima for both YDC15 and BCY15, making their segmentation impossible from image analyses. Moreover, an enlarged zone of an image (CM fabricated by dip coating; figure 24a) shows that the transition between the three phases is in the range of the image resolution (figure 24b). Insofar as phases proportion is very sensitive to the threshold position, the latter being limited by the resolution, the separation might be possible but will be error-prone. To counter act this difficulty, the idea consists in determining the grey level distribution characteristic of each material. Indeed, the grey level of each pixel in the image will allow for identifying to which material it corresponds. In other word, a phase map in grey level should be extracted from each image so that the correct proportion of BCY15 and YDC15 must be obtained.
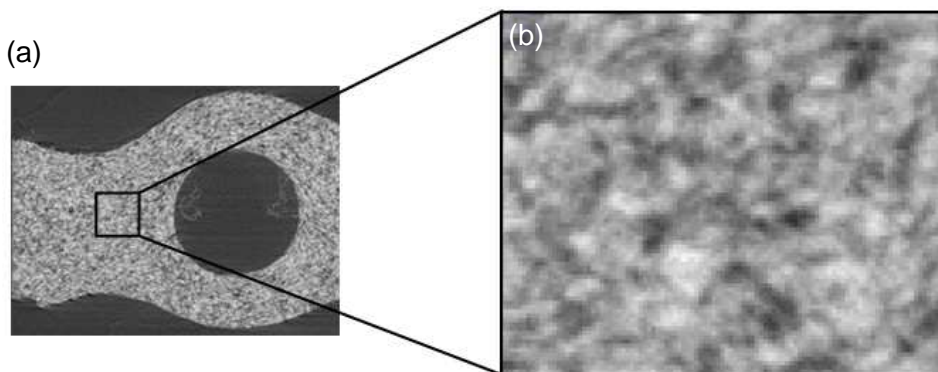

Figure 24. (a) Image recorded at the ESRF and (b) zoom in on a selected zone showing the resolution limit.

Knowing the grey level histogram of a BCY15 sample and the one of a composite central membrane, which composition is well-known, it is possible to extract the histogram of a pure YDC15 sample (figure 25). Indeed, the composite histogram is built up from the convolution of x% YDC15 and (1-x)% BCY15; as the histogram of pure BCY15 is accurately determined, the YDC15 one can be easily extracted (light grey line in figure 25) knowing the value x. On the one hand, thanks to this protocol,

---

[3] T.W. Ridler, S. Calvard, "Picture thresholding using an iterative selection method", IEEE Transactions on Systems, Man and Cybernetics **8** (1978) 630-632.

each pixel can be attributed to a phase according to its grey level, and the intersection between the YDC15 and BCY15 distributions corresponds to the uncertainty of the method. On the other hand, the threshold that defines the proportion of the two materials, the latter being known, can be changed iteratively until the experimental values are achieved. This latter operation was carried out to extract results from images recorded during the first ESRF session.
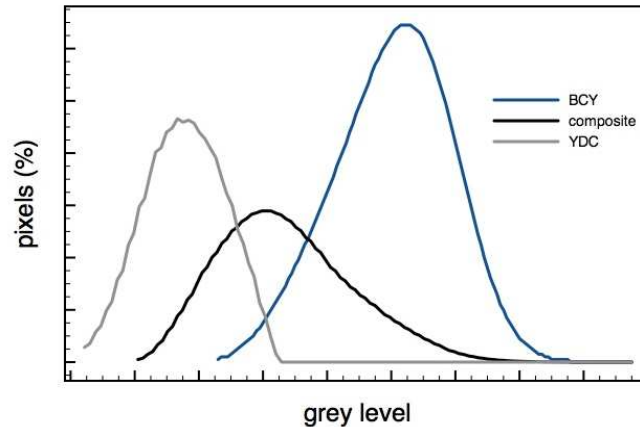

Figure 25. Histogram extracted from an image displaying the population of grey level for each material, BCY15 (dark blue line), YDC15 (light grey line) and the composite (black line).

V. Futur activities

As porosity percolation pathway and tortuosity are directly extracted from the 3D image analyses, these morphological parameters can be used to compare the ability of different microstructures to deal with flow and evacuation of water vapour in and out of the CM respectively. Computational Fluid Dynamics (CFD) calculations can be carried out in a representative volume element (RVE) whose the size is representative of the whole volume of the porous CM. VREs can be meshed and the calculations are performed using finite element method. This latter will be performed by introducing a peak of water vapour concentration C_o at $t = to$ and then calculating the distribution concentration C_{out} after it driving through the porous CM (figure 26); obviously, C_{out} will be closely dependant on the sample morphology in terms of tortuosity and percolation pathway.

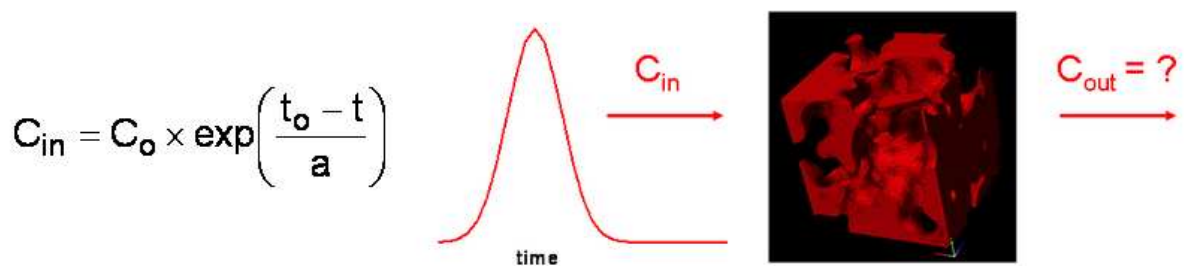$$C_{in} = C_o \times \exp\left(\frac{t_o - t}{a}\right)$$

Figure 26. CFD modelling strategy planned to investigate the water vapour evacuation out of the CM.

An estimation of 3D key parameters (free active surfaces, 3D tortuosity of pores or mixed conducting phases…) can be made on available 3D micrographs or on 3D simulations of microstructures, hence the prediction of the effective properties (Darcy permeability, effective anionic and protonic conductivities) via the implementation of the Morph-Hom code available at CMM of Mines ParisTech. In the case of simulated images, an optimization of the microstructure with respect to effective properties will be looked for, from a systematic exploration of the models parameters. On this basis, the potentialities of the novel components microstructure will be quantitatively known, and the most promising ones will be checked experimentally by back and forth between modelling and experimental results. In addition, numerical extraction of TPB segments from reconstruction of 3D X-ray microtomography images will be performed (figure 27a). The mirror 3D image of the active phases (figure 27a) displays the porous volume (figure 27b) in which circulation of water vapour can be modelled (figure 27c) using the CFD code of COMSOL.
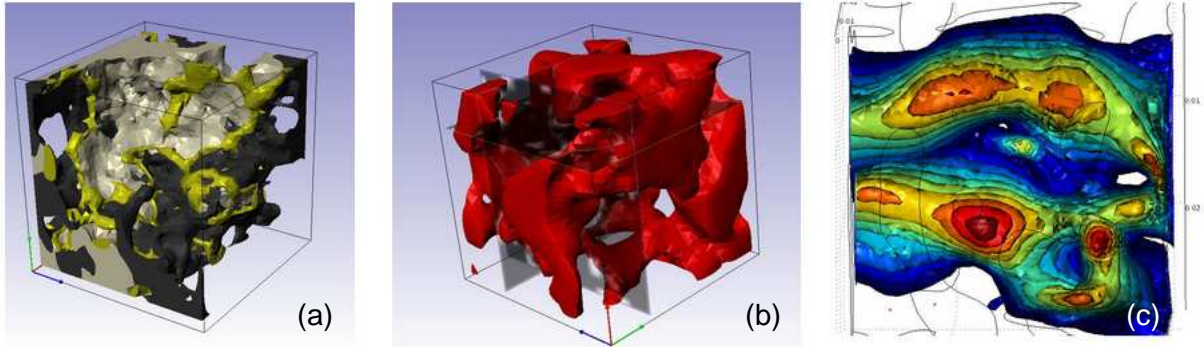
Figure 27. Results from the CMM. (a),(b) 3D reconstruction of the central membrane from X-ray microtomography experiments (green = TPB segments, dark grey = YDC15, ligh grey = BCY15, red = porosity); (c) CFD modelling of gradient of water vapour velocity inside the porous media of the CM.